ChemPubSoc Europe

DOI: 10.1002/open.201900172

Open Access ChemistryOPEN Full Papers

# Design and Testing of a Bending-Resistant Transparent Nanocoating for Optoacoustic Cochlear Implants

Alessandra Griffo,[a, b] Yingying Liu,[a] Riitta Mahlberg,[a] Hanna-L. Alakomi,[a] Leena-S. Johansson,[b] and Roberto Milani*[a]

A nanosized coating was designed to reduce fouling on the surface of a new type of cochlear implant relying on optoacoustic stimulation. This kind of device imposes novel design principles for antifouling coatings, such as optical transparency and resistance to significant constant bending. To reach this goal we deposited on poly(dimethylsiloxane) a PEO-based layer with negligible thickness compared to the curvature radius of the cochlea. Its antifouling performance was monitored upon storage by quartz crystal microbalance, and its resistance upon bending was tested by fluorescence microscopy under geometrical constraints similar to those of implantation. The coating displayed excellent antifouling features and good stability, and proved suitable for further testing in real-environment conditions.

## 1. Introduction

One of the main concerns in the design of biomedical implants is to achieve control over the interaction between biomaterial surfaces and the biological medium. Even though bioadhesion is part of the integration process of a biomaterial within the human body, it is of great importance to avoid non-specific protein and cell adhesion for example when prostheses[1] and scaffolds for tissue regeneration[2–4] are involved. This holds also in the case of cochlear implants, where adverse effects may include inflammation and fibrosis.[5–7] Recently a new operation mode was proposed for implantable cochlear devices, relying on laser irradiation to stimulate cochlear responses through the so-called *optoacoustic effect*.[8–10] For this type of implants one particularly undesirable event would be the growth of fibrous tissue on the surface of the device, which would interfere with light transmission and reduce its efficiency.[11,12]

Here we present an antifouling coating designed for one such device. In this new, highly miniaturized system an array of miniature lasers is placed inside the cochlea to provide optoacoustic stimulation, as described elsewhere in greater detail.[10] When designing a coating for this implant, several requirements need to be fulfilled. The first is to minimize protein and cell attachment in order to avoid biofilm formation, which might lead to infections and degradation of performance as described above. Clearly, it is also necessary for the antifouling action to persist over a long time scale in physiological conditions; there are however additional requirements which are specific to this particular type of device. It is evident for example that the coating needs to be transparent at the wavelength used for the optoacoustic stimulation, which is 1550 nm in the present case. Perhaps less obvious, but not any less important, is that the coating must be flexible enough to maintain its efficiency after implantation in the cochlea, whose typical spiral shape will result in the application of a continuous bending stress to the implant.[12]

In the past years there have been reports of cochlear implants based on protein repelling hydrogels[13] and biodegradable polymers[12] which reduced the formation of connective tissue and improved the electrode-nerve interface. In the present study, a triethoxysilane-terminated polyethylene oxide with 44 ethylene oxide units (PEO44-TES) was used. PEO is known for its non-toxicity and biological inertness,[14] as well as for its ability to reduce protein adsorption and cell adhesion thanks to steric repulsion and low hydrated interface free energy.[15–18] The length of the PEO chain was chosen to provide good surface coverage, while the alkoxysilane function is expected to allow stable covalent grafting onto the polydimethylsiloxane (PDMS) surface of the device after plasma activation (Figure 1). It is known that a number of more complex compositions and preparation methods have been reported in literature for antifouling coatings, including various modifications of PDMS, block copolymers, star-shaped polymers, polyelectrolyte multilayers and polymer brushes grown *in situ*.[12,19–25] In the context of a wider study which included different coating designs and deposition methods, however, here we wished to explore the possibility to use a nanosized polymer layer deposited by a simple, non-laborious *grafting to* approach. This might lead to somewhat lower coating densities, however it was reported before that highly dense, partly crosslinked polymer brush coatings can suffer from delamination due to osmotic pressure effects.[26] For coatings subject to significant bending stress, a lower density and a very small thickness

[a] A. Griffo, Y. Liu, R. Mahlberg, Dr. H.-L. Alakomi, Dr. R. Milani
VTT Technical Research Centre of Finland Ltd., P.O. Box 1000, FI-02044VTT, Espoo, Finland
E-mail: roberto.milani@vtt.fi
[b] A. Griffo, Dr. L.-S. Johansson
Department of Bioproducts and Biosystems, Aalto University, P.O. Box 16100, FI-00076Aalto, Espoo, Finland

Supporting information for this article is available on the WWW under https://doi.org/10.1002/open.201900172

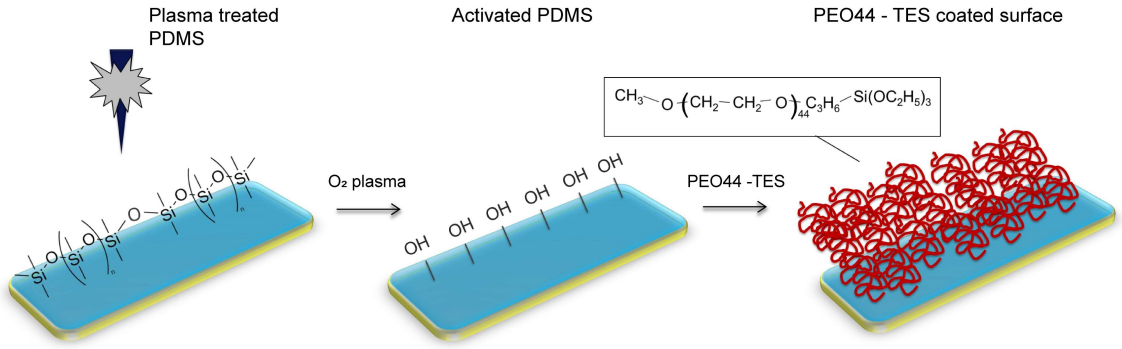


**Figure 1.** Schematic representation of the surface functionalization procedure. The PDMS surface was first treated by plasma, then PEO44-TES was covalently grafted.

compared to the applied radius of curvature may therefore be beneficial and lead to a satisfactory trade-off between performance and stability.

As a first step in this exploratory study, the PEO44-TES coating was deposited on PDMS surfaces to evaluate features such as optical transparency and *in vitro* antifouling performance towards single protein solutions, fibroblasts and bacteria. The antifouling features, in particular, were studied by Quartz Crystal Microbalance with Dissipation monitoring (QCM-D), which is a useful method to evaluate adsorption phenomena on polymer surfaces,[27,28] including those involving biological molecules.[29] Our results show that the proposed coating has high transparency and very good antifouling properties, which are mostly maintained even upon application of significant bending stress. The main focus here is to obtain information on the compositional, structural and functional stability of the coatings upon storage and bending. This will provide a basis for studies in conditions closer to the real application, and for a comparison with more complex coating designs, including *grafting from* approaches, which will be the object of separate publications.

## 2. Results and Discussion

### 2.1. Coating Characterization

The coating described in this work is expected to cover also the optical windows of the optoacoustic device, through which the radiation used for stimulation is transmitted.[10] The coating therefore needs to be transparent at the operating wavelength of the device, which is in the near infrared at 1550 nm. The first test performed was an assessment of the optical transmission features of PEO44-TES, which was deposited on glass slides to prepare a high density silane coating. The film was essentially transparent in the 900–2000 nm wavelength range, with a transmission value of ca. 98% at 1550 nm (Figure S1), therefore PEO44-TES satisfies the optical transparency requirements of the optoacoustic device.

The compositional and structural features of the coatings were characterized after its deposition on 600 μm-thick PDMS slides, i.e. the same encasing material and thickness planned for the implant. The substrate surface was first activated by oxygen plasma to allow covalent binding of PEO44-TES, monitoring the effectiveness and durability over time of the activation effect by water contact angle (WCA) measurement (Figure 2a). As expected, the plasma-treated PDMS was highly hydrophilic. The WCA was 9° after 30 minutes from treatment and rose to about 44° within the first two hours, after which it increased more slowly. The original value displayed by untreated PDMS was eventually recovered in two days. This is in good agreement with previous literature,[30,31] and is due to the PDMS polymer chains rearranging to minimize surface energy. Based on these data, in following experiments the functionalization with PEO44-TES was performed always within one hour from plasma activation.

The successful deposition of PEO was assessed by XPS elemental analysis. An increase in oxygen and a slight decrease in Si content were observed, which are consistent with the PDMS surface being covered by new, oxygen-rich polymer layers (Table 1). Most importantly, a new component appeared

**Table 1.** XPS elemental analysis for untreated and PEO44-TES coated PDMS. On the right side of the Table are reported the components of the C 1s peak, together with their respective percentage contribution to the whole peak.

| Sample | Elemental analysis (%) | | | | C 1s components (%) | | |
|---|---|---|---|---|---|---|---|
| | C 1s | O 1s | Si 2p | other | C–O | C–C C–Si | C–C[a] |
| PDMS | 44.9 | 24.5 | 30.6 | – | – | 86.4 | 13.6 |
| PEO44-TES | 39.3 | 34.2 | 26.3 | Na 1 s: 0.2 | 32.5 | 67.5 | – |

[a] This CC component is likely due to surface contamination.

in the C1s peaks which is compatible with C–O bonds and constitutes a strong indication of the presence of PEO (Figure 2c). For a hypothetical multilayer coating composed only by fully hydrolysed PEO44-TES, devoid of contaminants and with a thickness well above the penetration depth of XPS analyses (roughly 10 nm), the expected percentage of Si in the elemental analysis should be below 1%. Similarly, the distribution of C–O and C–C/C–Si components of the C 1s peak should be close to

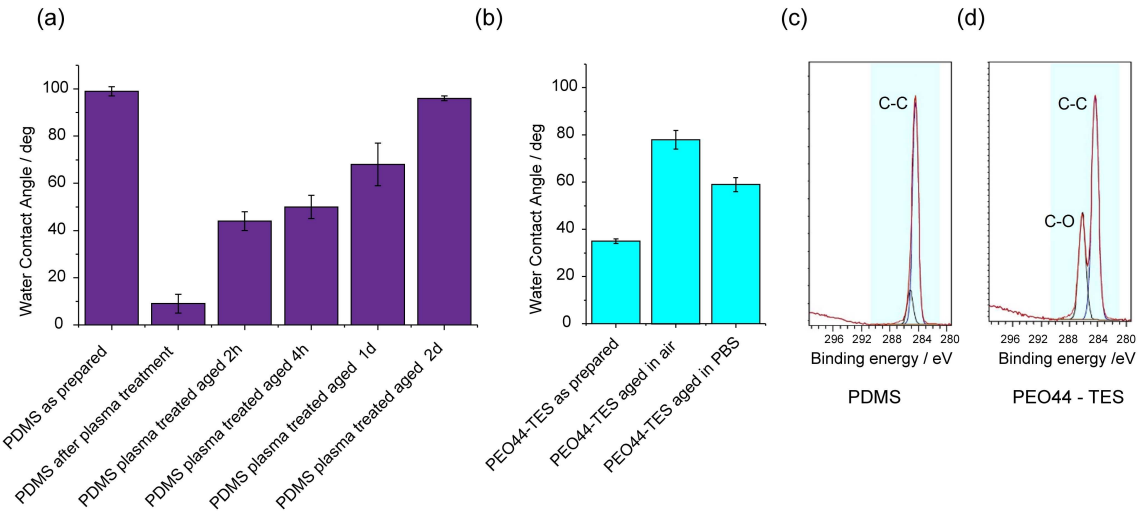


**Figure 2.** WCA of plasma-treated PDMS surfaces at different times after preparation (a), and of the PEO44-TES coating aged by storage for 4 weeks in dry and wet state (b). C1s XPS spectra for PDMS surfaces, both unmodified (c) and coated with PEO44-TES (d).

98% and 2% respectively, even assuming a random orientation of PEO44-TES in the layer.

The data reported in Table 1 for our coated surfaces are clearly distant from these values, as the percentage of Si decreased only from 30.6% to 26.3% upon coating deposition, and the contribution of the C–O component to the C 1s peak is estimated to be only 32.5%. This result is however not surprising. The average length of an ethylene oxide unit has been calculated to be about 0.28 nm, in helical ttg configuration and in the crystalline state.[32] In a fully extended helical configuration, therefore, the length of PEO44-TES would be close to 13 nm; for a non-dense monolayer in the dry state, where PEO chains can be expected to assume a collapsed configuration, the average thickness of the coating will thus be well below the maximum probing depth of XPS. This is also in line with the fact that no clear PEO-related peaks could be identified by FTIR-ATR analysis, which typically has a probing depth of the order of the micron (Figure S2). In addition, these results may be also due to the presence on the surface of residual uncrosslinked low molecular weight PDMS left from the preparation of the substrate, which cannot be ruled out as explained below in more detail.

The measurement of WCA can also give a first indication of the stability of the coating in dry and wet environments.[33] To do so, we compared the WCA of PDMS samples functionalized with PEO44-TES right after deposition, and after four weeks of storage in air and in physiological saline solution (0.85% NaCl, Figure 2b).

Freshly prepared PEO44-TES coatings displayed a WCA of 35°, which is in reasonable accord with literature values reported for analogous surfaces.[30,33] After four weeks aging, the WCA increased by ca. 24 degrees (from 35° to 59°) in physiological saline solution and by ca. 43 degrees (from 35° to 78°) in air (Figure 2b). This is a different behaviour from the one observed by Desai and coworkers, who reported that the WCA of PEO coatings deposited on silicon surfaces remained stable over 4 weeks of storage in saline buffer.[33] The difference may be explained by the different substrate material and deposition methods used. In our case it is possible that one portion of the exposed hydrophilic functions generated by plasma activation remained unreacted during coating deposition, and was later replaced by non-activated, hydrophobic PDMS as the polymer chains rearranged to minimize surface energy. It is however also possible that very small amounts of uncrosslinked, low molecular weight PDMS precursor residues from the curing process were released over time, as shown in previous literature,[34] since even very small amounts of these compounds might have a substantial effect on the measured WCA. Both hypotheses are consistent with the observation that the WCA increased more after storage in air, which is a more hydrophobic medium than the saline solution. Neither of these phenomena could have occurred in the system studied by Desai, since silicon is much more rigid and structurally stable than PDMS.

Some evolution of the coating morphology was also observed over time, as shown in Figure 3 by the AFM micrographs of Quartz Crystal Microbalance (QCM) sensors with a PDMS top layer before and after deposition of PEO44-TES. The freshly prepared coatings (Figure 3d,e) displayed gaps of a few hundred nm in size, within an otherwise dense layer showing ca. 4 nm high features (Figure 3f). This is most likely due to the presence of defects in the PDMS layer already before functionalization, as can be observed in Figure 3a,b.

After one month of storage in physiological saline solution, it was found that the surface of the film had undergone significant reconstruction (Figure 3g,h). The sample consistently displayed grooves with a depth of approximately two nanometers, and a general reduction of surface roughness (Figure 3i). Interestingly, similar patterns are often observed after exposing block copolymer films to solvents or vapours with significantly different affinity for the various blocks.[35–37] It could be hypothesized then that the structure observed here arises

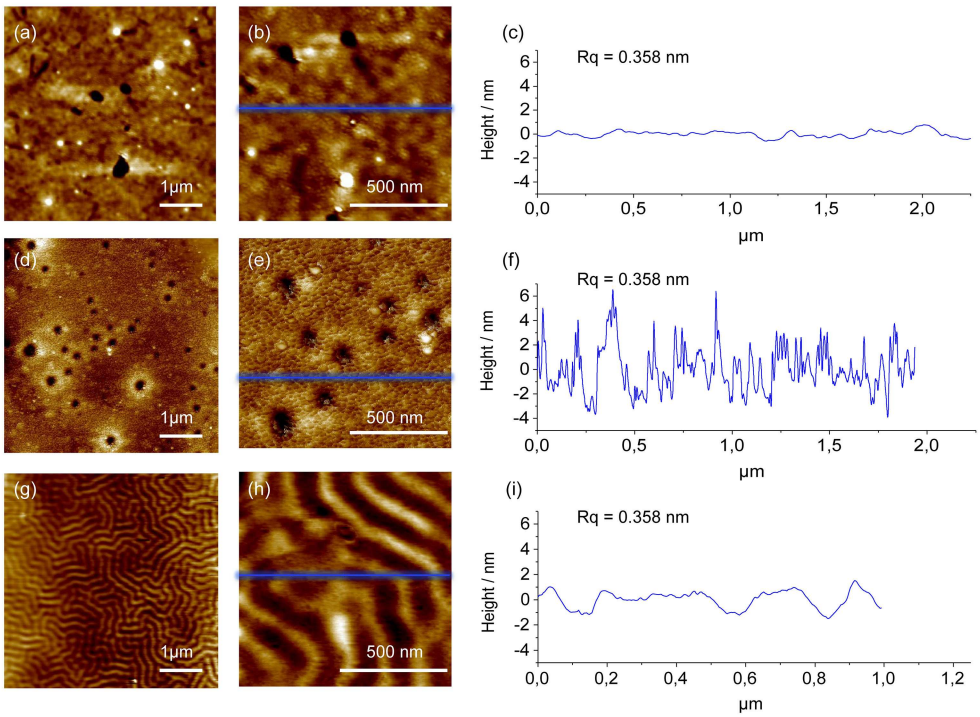


**Figure 3.** AFM micrographs of PDMS coated QCM sensors as such (a,b) and modified with PEO44-TES before (d, e) and after (g, h) aging for one month in physiological saline solution. Section analysis along the indicated blue lines are reported in panels (c), (f), (i).

from the surface microphase separation of hydrophilic PEO and hydrophobic PDMS domains in the top layer of the material, covalently bound but still retaining significant mobility. It should also be noted that the flattening observed for the aged coating could be beneficial to its antifouling performance, since surface roughness has been sometimes associated with improved cell adhesion.[38,39]

### 2.2. Protein Adhesion Tests

The PDMS surfaces modified with PEO44-TES appear to evolve over time to some degree, both from the compositional and structural points of view; it becomes then necessary to verify whether these changes affect the antifouling performance of the coating or not. To do this, we studied the adsorption of the two model proteins fibrinogen (Fg) and bovine serum albumin (BSA) by QCM-D. Although it has been reported that the performance of an antifouling surface may be different for the adsorption of single proteins compared to more complex biological media,[40] these data can still provide a useful and straightforward basis for a first evaluation of coating stability, both over time and upon bending.

QCM sensors with a PDMS top layer were coated with PEO44-TES in the same way as the PDMS slides, and exposed to 1 mg mL$^{-1}$ solutions of Fg and BSA. The Sauerbrey model[41,42] was used to estimate the mass adsorbed on the surface of these samples, since frequency and dissipation shifts were very small and little to no overtone splitting was observed. The viscoelastic Voigt model[43] was used instead to estimate the protein adsorbed on the surface of uncoated PDMS, where frequency and dissipation shifts were large and significant overtone splitting occurred. The QCM-D sensorgrams for both frequency and dissipation shifts are shown in Figure S3 in the Supporting Information.

The frequency/dissipation ($\Delta f$ vs. D) curves for Fg adsorption reported in Figure S4 show always a nearly linear dependence between the two shifts, however their slopes differ significantly depending on the type of surface. The value of $\Delta f/\Delta D$ is ca. 13 on uncoated PDMS, where thick protein layers are formed, and ca. 5 on PEO44-TES coatings, where very little Fg adsorption occurs. This suggests that the protein layer is highly hydrated.[44] Interestingly, two distinct slopes were found for BSA adsorption on uncoated PDMS, where $\Delta f/\Delta D$ is initially ca. 2.5 and then rapidly switches to ca. 12, which is closer to the value observed for fibrinogen. It is not straightforward to give an explanation for this result, however the adsorption of BSA seems to occur differently from that of Fg, at least in its initial stages. A meaningful frequency/dissipation chart could not be drawn for BSA adsorption on PEO44-TES, since the recorded shifts were too small compared to experimental noise.

The QCM-D experiments clearly showed that protein adsorption was strongly reduced on samples coated with PEO44-TES. The estimated adsorbed mass of Fg on uncoated PDMS was close to 3000 ng/cm$^2$, which is in reasonable accord with the one found by Nan and coworkers for adsorption on gold at the same protein concentration.[44] On the coated surface this value dropped to 170 ng/cm$^2$, which corresponds to

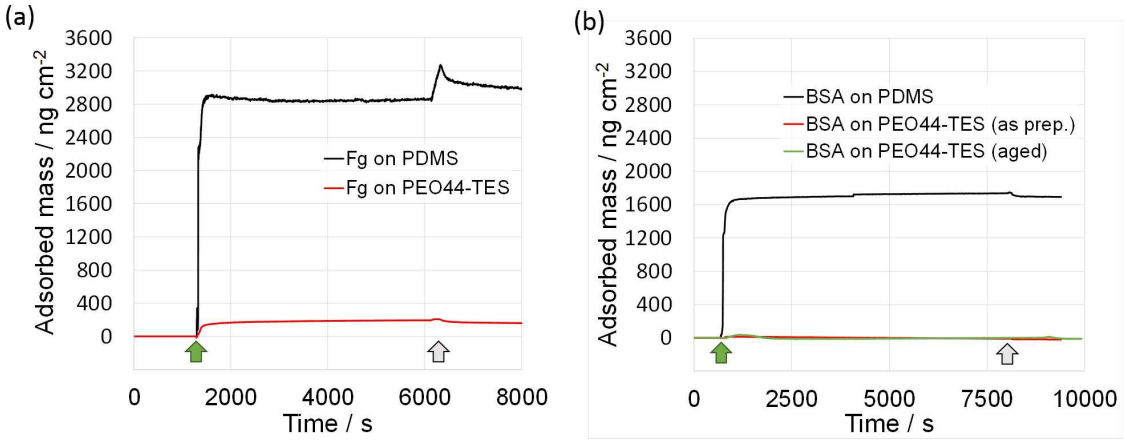


**Figure 4.** QCM-D data showing the adsorption of Fg (a) on virgin PDMS (black line) and on PEO44-TES coating (red line); and of BSA (b) on virgin PDMS (black line) and on PEO44-TES coating before and after aging in saline solution for 2 months (red and green line, respectively). Protein injection is marked by green arrows and PBS rinsing by grey arrows.

over 90% reduction of protein adsorption (Figure 4). In proportion the reduction was even stronger for BSA, whose estimated adsorbed mass went from 1730 ng/cm$^2$ on uncoated PDMS to nearly zero on surfaces modified with PEO44-TES. There is a significant difference in the adsorbed masses of Fg and BSA on uncoated PDMS; again, this is consistent with previous literature,[45,46] and can be explained by comparing the molecular weights and isoelectric points of the two proteins (for Fg, MW = 340 kDa and pI = 5.8; for BSA, MW = 66.5 kDa and pI = 4.8–5.0). Besides being a larger protein, Fg has an isoelectric point which is closer to the neutral pH used in the QCM-D experiments, and therefore is more prone to forming multilayers.

From the results shown, it is evident that the PEO44-TES coating is effective at preventing the adsorption of both proteins. The reasons for the antifouling properties of PEO have been discussed at length in literature and will not be examined in depth here, but they correlate with the enthalpic barrier which needs to be overcome to desorb interfacial water bound to PEO and make room for protein adsorption.[40,47,48]

As mentioned above, the AFM and WCA studies showed that changes occurred in the samples upon storage. However, when a PDMS surface coated with PEO44-TES and aged in physiological saline solution for 2 months was tested for BSA adsorption, the antifouling properties were still very similar to those of a freshly prepared sample (Figure 4b, green curve). Therefore the single-protein repellency features of the coating were maintained, in spite of the observed changes in structure and wettability. The stability of the PEO44-TES coating may be partially attributed also to some degree of crosslinking which is likely to occur thanks to its alkoxysilane molecules.

### 2.3 Cell Adhesion Tests

A preliminary evaluation of the ability of the coating to prevent cell adhesion was also performed, by incubating both coated and uncoated samples in bacterial and fibroblast cultures. A mixture of *Staphylococcus aureus*, *Staphylococcus epidermis* and *Pseudomonas aeruginosa* was used for the bacterial growth tests. Uncoated PDMS surfaces already showed relatively low bacterial viability under the conditions of the study, with only 2.9 Log colony forming units (CFU) per square centimetre. A clear improvement was nonetheless observed after deposition of PEO44-TES, as this value dropped to 1.8 Log CFU cm$^{-2}$.

For the fibroblast adhesion test, some representative images can be found in Figure 5. Cell clusters were easily identified on uncoated PDMS, while only very few fibroblasts could be found on the PEO44-TES surfaces. It should be noted that a rather small number of clearly identifiable fibroblasts was found also in some of the uncoated PDMS repeats. In these cases however surface fouling was still an issue since considerable amounts of

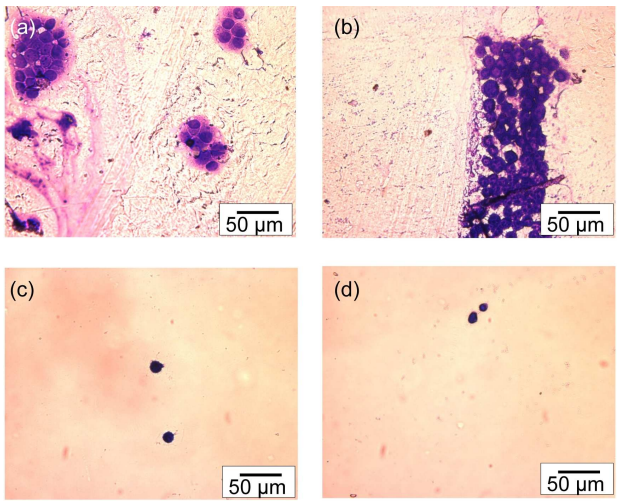


**Figure 5.** Optical microscope images of PDMS surfaces incubated with fibroblasts: uncoated PDMS (a,b), PEO44-TES coated PDMS (c,d).

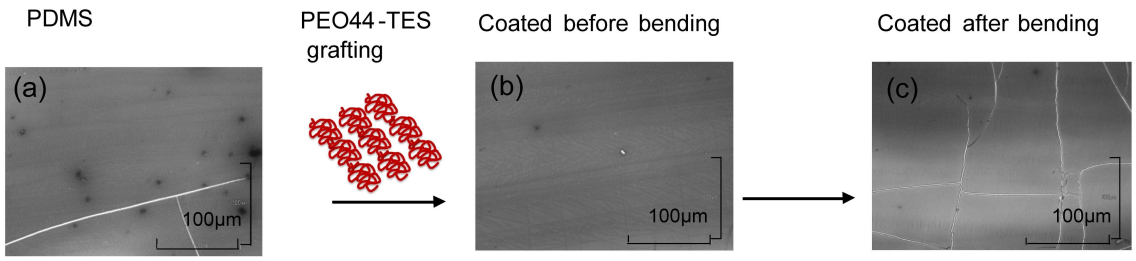


**Figure 6.** Optical microscope images of uncoated PDMS before bending (a), and of PEO44-TES coated PDMS before bending tests (b), and after bending, on the compression side (c). More images of the PEO44-TES coated PDMS after compression and extension are reported in Figure S6.

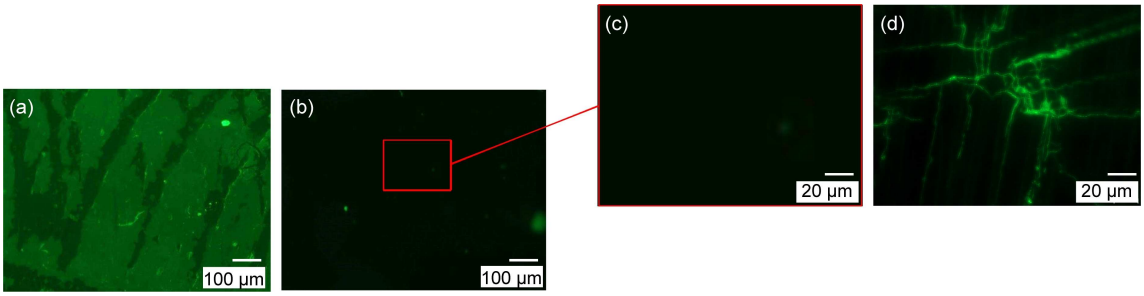


**Figure 7.** Epifluorescence images of surfaces incubated with BSA-FITC. Uncoated PDMS (a), PEO44-TES coating on PDMS and its magnified area before bending (b, c) and after bending, on the extension side (d). Brightness was increased by 50% for all images

cell debris were found scattered throughout the surfaces (data not shown), which suggests that cell damage may have occurred in those instances. In any case, it is important to remark that similar deposits were never observed on any of the samples coated with PEO44-TES. Overall, these results confirm that the coatings display a very good antifouling activity not only towards single protein adsorption, but also for cell adhesion *in vitro*.

### 2.4. Bending Resistance Tests

One of the main aims of this study was to investigate whether the coating maintains its functionality upon application of bending stresses. The intended use of the optoacoustic device requires the insertion of a flexible element into the cochlea, which has a spiral, snail shell-like shape with a curvature diameter of about 6 mm. The implanted device therefore is expected to experience continuous and significant bending stress throughout its operation lifetime. In order to reproduce these conditions, coated and uncoated PDMS slides having the same thickness planned for the implantable elements of the optoacoustic device (600 μm) were bent around a cylindrical mandrel bending tester with the same curvature diameter as an average cochlea (6 mm, Figure S5).

The samples were first analysed optical microscopy to verify the occurrence of cracks or other surface damage (Figure 6 and S6). Some cracks were visible after bending, both on the sides subject to compression and to extension deformation. However it is important to note that some small cracks were already visible on the pristine PDMS, before coating deposition or the application of any bending stress. These pre-existent cracks were probably formed during the fabrication of the PDMS substrates and it is reasonable to assume that they may extend when bending stress is applied. The presence of cracks after bending may therefore be a consequence of the PDMS fabrication process rather than of an intrinsic fragility of the PEO44-TES coatings, which are expected to be rather flexible on account of both their nature and very small thickness.

It is important for the surface of a cochlear implant to maintain its antifouling functionality at a reasonable level upon bending. In order to verify this, samples subjected to bending tests were also incubated with a solution of fluorescein-labelled BSA (BSA-FITC) and imaged on an epifluorescence microscope to verify whether protein adsorption occurred. This test was performed on the coatings before and after bending, as well as on pristine PDMS as a control. As expected the uncoated PDMS displayed a diffuse fluorescence signal, which was instead absent on the PEO44-TES coatings before bending (Figure 7a–c and Figure S7). The bent samples only showed some fluorescence along the cracked areas, particularly on the side subjected to extension stress (Figure 7d).

This suggests that the extension of pre-existent cracks upon bending as described above results in damaged areas, where uncoated PDMS is exposed and therefore protein adsorption can occur to some degree. As clearly shown by the images,

however, the fluorescent signal is strictly confined inside the cracks, so that no dramatic loss of the antifouling performance takes place overall. It is also worth noting that the operating mode of the bending tester is such that the stress applied to the samples is surely larger than the one expected for the implants upon insertion into the cochlea. This problem nevertheless could be reduced by improving the PDMS curing process in such a way as to reduce or avoid the formation of cracks in the first place. More epifluorescence images are available in the Supporting Information, for both the sides of the samples subject to extension and to compression (Figure S7).

## 3. Conclusions

In this work is reported the design and preliminary testing of a thin antifouling coating for a new type of cochlear implant, which is planned to provide optoacoustic stimulation from inside the cochlea. This particular application requires the coating not only to reduce protein and cell adhesion, but also to be transparent and maintain its performance under significant bending stress, as dictated by the small size and spiral-like shape of the cochlea.

The coating was prepared through a simple and scalable procedure in a way to possess negligible thickness compared to the cochlear radius, and displayed very good features in terms of optical transparency and antifouling action. Its presence prevented protein adsorption almost completely, and reduced significantly the adhesion of fibroblasts and bacteria. Some structural evolution of the surfaces was observed over time, which however did not affect their ability to lower protein adsorption even after storage in physiological saline solution for two months. A small amount of structural damage was revealed in bending tests, which however seemed to be due to defects occurring during fabrication of the PDMS substrate, rather than to an intrinsic flaw of the coating.

The results presented in this work indicate that the PEO44-TES coating is a potential candidate for antifouling protective layers on optoacoustic cochlear implants, and could be potentially used also for other biomedical applications. Further investigations will be necessary to clarify its performance and stability over longer periods and closer to actual operational conditions; these tests and the evaluation of more complex coating designs will be the object of future studies.

## Experimental Section

Polydimethylsiloxane (PDMS) sheets of size 20×60×0.6 mm (NuSil MED-6033 silicone elastomer) were kindly supplied by Dr. Rony Jose James in CSEM (Neuchâtel, Switzerland); the thickness of the slides was chosen to match the planned thickness of the implantable element (600 μm). Polyethylene oxide having a chain length of 44 monomer units with one methyl ether and one triethoxysilane termination (PEO44-TES) was purchased from Specific Polymers; bovine serum albumin (BSA), fibrinogen (Fg), albumin labelled with fluorescein isothiocyanate (BSA-FITC) and solvents were purchased from Sigma Aldrich.

*Silanization with PEO44-TES.* The functionalization procedure was adapted starting from previously reported methods.[30,49] Typically, three PDMS slides with size varying from 15×15 mm to 10×30 mm were sonicated in ethanol, acetone and Milli-Q water for 5 min each, then rinsed with acetone, ethanol and water, and dried with nitrogen. Sample surfaces were first activated by $O_2$ plasma treatment (Diener Nano Plasma) for 60 sec (pressure = 0.3 Torr, Power = 80–100 W).[50,51] Treatment parameters were chosen in order to limit surface damage.[52,53] Then, 0.150 g of PEO44-TES were dissolved in 15 mL of a mixture of ethanol:water (1 : 2 v/v), so as to achieve a final concentration of 10 mg mL$^{-1}$ (4.6 mM). The pH of the solution was adjusted at 2 by adding a few drops of 2 M HCl aqueous solution (pH checked with indicator strips). The activated PDMS slides were dipped into the solution within 1 h from plasma treatment and incubated in it overnight, then rinsed with a mixture of ethanol:water (1 : 2 v/v) and thoroughly with water, and finally dried under nitrogen flux.

*Optical transparency tests.* Optical absorption spectra were collected on a Perkin Elmer Lambda 900 spectrophotometer. The spectral acquisition range used was between 175 nm and 3300 nm. For these measurements, a PEO44-TES coating was prepared on glass slides (2 cm×4 cm) according to the same procedure described above for PDMS slides.

*Water contact angle (WCA).* Water contact angle (KSV CAM200, Biolin Scientific) was measured using the sessile drop method, with 5 μL water droplets. All reported values were the average of at least 3 measurements performed on different areas of the samples.

*X-ray photoelectron spectroscopy analysis (XPS).* XPS characterization was carried out on an AXIS Ultra instrument by Kratos. The films were placed in a sample holder with UHV compatible carbon tape and pre-evacuated overnight, together with an in situ reference sample of 100% ash-free cellulose filter paper. Monochromatic Al Kα irradiation at low irradiation (100 W) was used under neutralisation. Low resolution/wide energy range, and high resolution scans of C 1s, O 1s, N 1s and Si 2p regions were taken on at least three locations for each sample. The software CasaXPS™ was used for data analysis. The C 1s high resolution data was curve fitted with Gaussian components for a more detailed chemical analysis[54] and the binding energies of all spectra were adjusted with the help of the in-situ reference and the CC component present in all samples (i.e. carbon atoms without oxygen neighbours). Wide scans were used in surface elemental analysis.

*Fourier Transform infrared analysis (FT-IR).* FT-IR measurements (Nicolet iS50 FT-IR, ThermoScientific) were recorded in dry environment under total attenuated reflectance conditions by pressing the samples against the diamond crystal plate.

*Atomic force Microscopy (AFM).* Topographical images were acquired by atomic force microscopy (AFM) in tapping mode with a Digital Instruments Dimension 3100 Scanning Probe Microscope (Bruker, Santa Barbara, CA). Silicon cantilevers (NSC15/AIBS, MicroMasch, Tallinn Estonia) with a driving frequency around 300 − 360 kHz were used. Two different scan sizes were recorded: 1×1 μm$^2$ and 5×5 μm$^2$. All measurements were performed at room temperature and in air.

*Quartz Crystal Microbalance with Dissipation monitoring (QCM-D).* The QCM-D measurements were performed in flow mode using a Q-Sense E4 instrument and PDMS-coated quartz crystals with a fundamental frequency of 5 MHz (Biolin Scientific, Sweden). The measurements were carried out at 22 °C using a flow rate of 100 μL min$^{-1}$. PDMS-coated QCM-D sensors, both unmodified and

functionalized with PEO44-TES as described above, were stabilized in 10 mM phosphate buffer saline (pH 7), then exposed to 1 mg mL$^{-1}$ protein solutions in the same buffer until a constant frequency value was obtained, and finally rinsed with the running buffer. Further measurements were performed on sensors prepared in the same way after storing in physiological saline solution (0.85% NaCl) for 2 months. The data were analyzed with the Dfind software provided by the instrument manufacturer. Adsorbed mass values were estimated by using the viscoelastic Voigt model (Broadfind algorithm in Dfind) for protein layers on uncoated PDMS, and the Sauerbrey model for protein layers on PEO44-TES coatings (Composite Sauerbrey algorithm in Dfind). Harmonics 3, 5, 7, 9 and 11 were used for fitting, with density values of 1100 g L$^{-1}$ for the protein layers and 1006 g L$^{-1}$ for the bulk liquid.

*Fibroblast adhesion tests.* Mouse fibroblast strain NCTC clone 929 [L cell, L-929, derivative of Strain L] (ATCC© CCL-1™) was cultured in 25 cm$^2$ T-flasks in ATCC-formulated Eagle's Minimum Essential Medium, Catalog No. 20-2003 medium supplemented with 10% horse serum. Cells were cultured at 37 °C in a humidified atmosphere containing 5% $CO_2$ and routinely passaged by trypsinization. Three PDMS slides per each type of sample (unmodified and coated with PEO44-TES) were sterilized by immersion in 70% ethanol for 20 min, rinsed in sterile deionized water and dried inside a sterile hood. The slides were then put in 12-well polystyrene culture plates (one sample per well). A 0.3 mL aliquot of cell suspension ($1\times10^5$ cell mL$^{-1}$) in the supplemented medium was carefully layered onto each sample. All culture plates were then incubated in the $CO_2$ incubator for 3 hours and after incubation the medium was decanted and samples were rinsed twice with the supplemented medium to release unattached cells. All rinsing was done by shaking the culture plate for 10 s at 80 rpm on a plate shaker after addition of 1 mL of fresh medium into each well. Samples were fixed with 70% ethanol for 10 min and after decanting the ethanol they were stained with 0.4% crystal violet for 5 min. After staining the samples were rinsed with sterile water and air-dried. Images of the sample surfaces were collected on an Olympus microscope.

*Bacterial growth tests.* Bacterial adhesion and antimicrobial activity of the surfaces was examined against a microbial mixture of *Staphylococcus aureus* VTT E-70045, *Staphylococcus epidermis* VTT E-97768T and *Pseudomonas aeruginosa* VTT E-96728, in physiological salt solution (0.85% NaCl), and the results were presented as colony forming units (CFU) cm$^{-2}$. Target microbes were grown overnight in Tryptic Soy Broth (TSB) and diluted to obtain inoculum level $5\times10^3$–$10^4$ CFU mL$^{-1}$ for the antimicrobial activity testing. Heat-sterilized (160 °C, 4 h) test surfaces were submerged in glass vessels containing 200 mL of 0.85% NaCl solution and microbial inoculum. Samples were incubated at 37 °C with orbital shaking (50 rpm). The number of viable bacteria was analysed by plate count analysis on Plate count agar (PCA). Three replicates of each sample type (coated and uncoated) were placed in 45 mL peptone saline solution and cells were released from the surface by sonication (10 min at room temperature). A subsample was homogenized by mixing with Vortex (1 min) and after dilution series plated on Plate count agar.

*Bending Tests.* Mechanical tests were performed on a cylindrical mandrel bending tester (Model 266 S ERICHSEN) using a mandrel with a curvature diameter of 6 mm. The functionalized PDMS slides (10×60×0.6 mm) were bent around the mandrel and kept in position for 15 s. After that, they were removed from the instrument and imaged by optical microscopy (Nikon Eclipse 50i) using 10× and 40× magnifications on both the extended and compressed sides.

*Fluorescence microscopy.* Fluorescence tests were carried out on the PEO44-TES coatings before and after bending tests. Briefly, 200 µL of 0.5 mg mL$^{-1}$ BSA-FITC ($\lambda$ of excitation at 495 nm and $\lambda$ of emission at 517 nm) in 10 mM PBS (pH 7) were drop-cast on all samples and allowed to incubate for 120 minutes. After that the samples were rinsed thoroughly with water, dried under $N_2$ flux and imaged at the fluorescence microscope (ZEISS AxioImager Z2, Apotome). The same exposure time was used (600 ms) and objective lenses (10× and 40×) were used were for all recorded images.

## Acknowledgements

*The authors would like to acknowledge financial support from the European Commission under the Seventh Framework Programme (ACTION project, grant agreement no. 611230) and all the partners involved in the ACTION project, particularly Dr. Rony Jose James and Dr. Mark Fretz (CSEM, Neuchâtel, Switzerland) for supplying the PDMS substrates and Dr. A. Rettenmaier (Hannover Medical School, Germany) for fruitful discussions. R. Mi. and Y. L. also gratefully acknowledge the Academy of Finland for funding (project SelfSmart, decision no. 276537 and 284508).*

## Conflict of Interest

The authors declare no conflict of interest.

**Keywords:** antifouling coatings · implantable devices · interfaces · silanes · surface chemistry · thin films

[1] R. Pérez-Tanoira, X. Han, A. Soininen, A. A. Aarnisalo, V.-M. Tiainen, K. K. Eklund, J. Esteban, T. J. Kinnari, *J. Biomed. Mater. Res.* **2017**, *105*, 62–72.
[2] B. B. Mandal, S. C. Kundu, *Biomaterials* **2009**, *30*, 2956–2965.
[3] J. L. Moreau, H. H. K. Xu, *Biomaterials* **2009**, *30*, 2675–2682.
[4] S. Deville, E. Saiz, R. K. Nalla, A. P. Tomsia, *Science* **2006**, *311*, 515–518.
[5] J. Fayad, F. H. Linthicum, F. R. Galey, S. R. Otto, W. F. House, *Ann. Otol. Rhinol. Laryngol.* **1991**, *100*, 807–811.
[6] J. B. Nadol, D. K. Eddington, *Otol. Neurotol.* **2004**, *25*, 257–262.
[7] M. A. Somdas, P. M. M. C. Li, D. M. Whiten, D. K. Eddington, J. B. Nadol, *Audiol. Neuro-Otol.* **2007**, *12*, 277–284.
[8] K. Y. Zhang, G. I. Wenzel, S. Balster, H. H. Lim, H. Lubatschowski, T. Lenarz, W. Ertmer, G. Reuter, *Opt. Express* **2009**, *17*, 23037–23043.
[9] N. Kallweit, P. Baumhoff, A. Krueger, N. Tinne, A. Kral, T. Ripken, H. Maier, *Sci. Rep.* **2016**, *6*, 28141.
[10] S. Mohrdiek, M. Fretz, R. J. James, G. S. Durante, T. Burch, A. Kral, A. Rettenmaier, R. Milani, M. Putkonen, W. Noell, et al., in *Proc. of SPIE Vol*, **2017**, pp. 100520 K–1.
[11] G. I. Wenzel, S. Balster, K. Zhang, H. H. Lim, U. Reich, O. Massow, H. Lubatschowski, W. Ertmer, T. Lenarz, G. Reuter, *J. Biomed. Opt.* **2009**, *14*, 044007—044007-6.
[12] A. Wrzeszcz, M. Steffens, S. Balster, A. Warnecke, B. Dittrich, T. Lenarz, G. Reuter, *J. Biomed. Mater. Res.* **2015**, *103*, 169–178.
[13] P. Ceschi, A. Bohl, K. Sternberg, A. Neumeister, V. Senz, K. P. Schmitz, M. Kietzmann, V. Scheper, T. Lenarz, T. Stöver, et al., *J. Biomed. Mater. Res. Part B Appl. Biomater.* **2014**, *102*, 1255–1267.
[14] N. A. Alcantar, E. S. Aydil, J. N. Israelachvili, *J. Biomed. Mater. Res.* **2000**, *51*, 343–351.
[15] A. Michelmore, P. Gross-Kosche, S. A. Al-Bataineh, J. D. Whittle, R. D. Short, *Langmuir* **2013**, *29*, 2595–2601.
[16] Y. Li, B. W. Muir, C. D. Easton, L. Thomsen, D. R. Nisbet, J. S. Forsythe, *Appl. Surf. Sci.* **2014**, *288*, 288–294.

[17] M. Shen, M. S. Wagner, D. G. Castner, B. D. Ratner, T. A. Horbett, *Langmuir* **2003**, *19*, 1692–1699.
[18] S. I. Jeon, J. H. Lee, J. D. Andrade, P. G. De Gennes, *J. Colloid Interface Sci.* **1991**, *142*, 149–158.
[19] M. S. Selim, M. A. Shenashen, S. A. El-Safty, S. A. Higazy, M. M. Selim, H. Isago, A. Elmarakbi, *Prog. Mater. Sci.* **2017**, *87*, 1–32.
[20] M. S. Selim, S. A. El-Safty, N. A. Fatthallah, M. A. Shenashen, *Prog. Org. Coat.* **2018**, *121*, 160–172.
[21] M. S. Selim, A. Elmarakbi, A. M. Azzam, M. A. Shenashen, A. M. EL-Saeed, S. A. El-Safty, *Prog. Org. Coat.* **2018**, *116*, 21–34.
[22] M. S. Selim, M. A. Shenashen, A. Elmarakbi, N. A. Fatthallah, S. Hasegawa, S. A. El- Safty, *Chem. Eng. J.* **2017**, *320*, 653–666.
[23] B. Zhu, T. Eurell, R. Gunawan, D. Leckband, *J. Biomed. Mater. Res.* **2001**, *56*, 406–416.
[24] I. Wong, C.-M. Ho, *Microfluid. Nanofluid.* **2009**, *7*, 291.
[25] J. Groll, J. Fiedler, E. Engelhard, T. Ameringer, S. Tugulu, H.-A. Klok, R. E. Brenner, M. Moeller, *J. Biomed. Mater. Res.* **2005**, *74A*, 607–617.
[26] S. Tugulu, H.-A. Klok, *Biomacromolecules* **2008**, *9*, 906–912.
[27] M. A. Shenashen, T. Okamoto, M. Haraguchi, *Reactive and Functional Polymers* **2011**, *71*, 766–773.
[28] M. A. Shenashen, M. M. Ayad, N. Salahuddin, M. A. Youssif, *Reactive and Functional Polymers* **2010**, *70*, 843–848.
[29] M. A. Shenashen, K. K. Shenashen, *Nova Publisher* **2013**, 213–228.
[30] S. Jo, K. Park, *Biomaterials* **2000**, *21*, 605–616.
[31] P. Harder, M. Grunze, R. Dahint, G. M. Whitesides, P. E. Laibinis, *J. Phys. Chem. B* **1998**, *102*, 426–436.
[32] F. Oesterhelt, M. Rief, H. E. Gaub, *New J. Phys.* **1999**, *1*, 6–6.
[33] S. Sharma, R. W. Johnson, T. A. Desai, *Langmuir* **2004**, *20*, 348–356.
[34] J. N. Lee, C. Park, G. M. Whitesides, *Anal. Chem.* **2003**, *75*, 6544–6554.
[35] P. Busch, D. Posselt, D.-M. Smilgies, B. Rheinländer, F. Kremer, *Macromolecules* **2003**, *36*, 8717–8727.
[36] R. A. Farrell, T. G. Fitzgerald, D. Borah, J. D. Holmes, M. A. Morris, *Int. J. Mol. Sci.* **2009**, *10*, 3671–3712.
[37] R. Lundy, S. P. Flynn, C. Cummins, S. M. Kelleher, M. N. Collins, E. Dalton, S. Daniels, M. A. Morris, R. Enright, *Phys. Chem. Chem. Phys.* **2017**, *19*, 2805–2815.
[38] N. J. Hallab, K. J. Bundy, K. O'Connor, R. L. Moses, J. J. Jacobs, *Tissue Eng.* **2001**, *7*, 55–71.
[39] D. P. Dowling, I. S. Miller, M. Ardhaoui, W. M. Gallagher, *J. Biomater. Appl.* **2011**, *26*, 327–347.
[40] T. Riedel, Z. Riedelová-Reicheltová, P. Májek, C. Rodriguez-Emmenegger, M. Houska, J. E. Dyr, E. Brynda, *Langmuir* **2013**, *29*, 3388–3397.
[41] G. Sauerbrey, *Z. Physik* **1959**, *155*, 206–222.
[42] F. Hook, M. Rodahl, B. Kasemo, P. Brzezinski, *Proc. Natl. Acad. Sci. USA* **1998**, *95*, 12271–12276.
[43] M. V. Voinova, M. Rodahl, M. Jonson, B. Kasemo, *Phys. Scr.* **1999**, *59*, 391–396.
[44] L. Guicai, S. Xiaoli, Y. Ping, Z. Ansha, H. Nan, *Solid State Ionics* **2008**, *179*, 932–935.
[45] L. M. Pandey, S. K. Pattanayek, D. Delabouglise, *J. Phys. Chem. C* **2013**, *117*, 6151–6160.
[46] K. Y. Chumbimuni-Torres, R. E. Coronado, A. M. Mfuh, C. Castro-Guerrero, M. Fernanda Silva, G. R. Negrete, R. Bizios, C. D. Garcia, *RSC Adv.* **2011**, *1*, 706–714.
[47] R. L. C. Wang, H. J. Kreuzer, M. Grunze, *J. Phys. Chem. B* **1997**, *101*, 9767–9773.
[48] M. Morra, *J. Biomater. Sci. Polym. Ed.* **2000**, *11*, 547–569.
[49] S. Gauthier, J. P. Aimé, T. Bouhacina, A. J. Attias, B. Desbat, *Langmuir* **1996**, *12*, 5126–5137.
[50] P. G. Vahey, S. A. Smith, C. D. Costin, Y. Xia, A. Brodsky, L. W. Burgess, R. E. Synovec, *Anal. Chem.* **2002**, *74*, 177–184.
[51] V. Sharma, M. Dhayal, Govind, S. M. Shivaprasad, S. C. Jain, *Vacuum* **2007**, *81*, 1094–1100.
[52] Y. Yang, K. Kulangara, R. T. S. Lam, R. Dharmawan, K. W. Leong, *ACS Nano* **2012**, *6*, 8591–8598.
[53] A. Tserepi, E. Gogolides, K. Tsougeni, V. Constantoudis, E. S. Valamontes, *J. Appl. Phys.* **2005**, *98*, 113502.
[54] G. A. George, *Polym. Int.* **2003**, *33*, 439–440.

Manuscript received: May 16, 2019